# Excited-State Dynamics of *trans,trans*-Distyrylbenzene: Transient Anisotropy and Excitation Energy Dependence

**Feng-Cheng Hsu,[†] Michitoshi Hayashi,[*,‡] Houng-Wei Wang,[‡] Sheng Hsien Lin,[†,§] and Juen-Kai Wang[*,‡,§]**

*Department of Chemistry, National Taiwan University, Taipei, Taiwan 106, Center for Condensed Matter Sciences, National Taiwan University, Taipei, Taiwan 106, and Institute of Atomic and Molecular Sciences, Academia Sinica, Taipei, Taiwan 106*

*Received: August 16, 2006; In Final Form: December 10, 2006*

We report a study of excited-state dynamics of *trans,trans*-distyrylbenzene in hexane solution with femtosecond two-color transient absorption spectroscopy. A consistent model of two distinct excited states, $S_1$ and X, connected by the 10 ps dynamics is proposed with the support from the analysis of excited-state anisotropy. An investigation on the 10 ps dynamics with varying excitation energy has been also conducted. In the assumption of fast intramolecular vibrational redistribution, a dependence of this nonradiative 10 ps process on intramolecular temperature in the $S_1$ state has been analyzed. We have found that an effective mode of $\sim$1270 $cm^{-1}$ is responsible for the 10 ps dynamics. The analysis of both anisotropy and pump-dependent results further implies that a distribution of rotamers may exist in the X state. The result indicates a drastic different excited-state relaxation pathway than that of *trans*-stilbene.

## 1. Introduction

Poly(*p*-phenylenevinylene) (PPV) and its derivatives have attracted much attention in the field of polymer light emitting devices since the 1990s.[1,2] One of the PPV oligomers, 1,4-distyrylbenznene (DSB), deserves deep investigation due to not only its potential in highly efficient emitting devices but also its relation to stilbene, which is the prototype molecule for photoisomerization.[3,4] Stilbene exhibits characteristic behaviors in its excited state. Especially, the existence of an energy barrier of $\sim$1200 $cm^{-1}$ in the $S_1$ state of *trans*-stilbene governs its primary step of photoisomerization before progressing to the so-called "phantom state" where the branching between trans- and cis-isomers occurs. The crossing of this energy barrier takes $\sim$100 ps depending on solvent temperature and viscosity. It is thus reasonable to ask whether these excited-state properties can be further extended to longer oligomers. *trans,trans*-DSB, as one of three DSB isomers, is a PPV oligomer that extends conjugation in the styryl group. It serves as the first candidate in studying the dependence of photophysical and photochemical properties on the molecular chain length in the PPV family.[5] Several recent studies have been focused on its steady-state photophysical properties and photoisomerization kinetics.[6−10] In contrast to the prototypical stilbene in which many detailed studies have been performed,[3,4] the excited-state dynamics of *trans,trans*-DSB in solution was investigated only recently by our group.[11]

In a previous ultrafast spectroscopic study on *trans,trans*-DSB,[11] we discovered that in the excited-state absorption spectrum an absorbance decrease at $\sim$740 nm and a simultaneous increase at $\sim$720 nm take place in 10 ps, which are assigned to the process transferring the initial excited-state population ($S_1$) to a distinct intermediate state. This 10 ps dynamics is still observed in the case of 0−0 excitation, which suggests that the vibrational relaxation assignment in the $S_1$ state is unlikely the origin.[11] In contrast, the evolution of the excited-state absorption spectrum of *trans*-stilbene shows spectral narrowing behavior that has been assigned to the vibrational relaxation process.[12,13] However, many questions still remain about this intermediate state. First, is there any other evidence to further support its existence? Second, how does its behavior depend on the excess energy in the first excited state? Finally, what role does it play in the photoisomerization dynamics of *trans,trans*-DSB? In this study, probe wavelength-dependent transient anisotropy was measured and analyzed. In addition, a theoretical calculation on *trans,trans*-DSB was performed to facilitate the interpretation. Finally, the dependence of the 10 ps process on the excitation wavelength was investigated to unravel the characteristics of this population transfer process.

## 2. Experimental and Computational Methods

The DSB sample was synthesized by the Wittig reaction,[14] producing a mixture of three isomers (*trans,trans*-, *cis,trans*-, and *cis,cis*-DSB). The pure *trans,trans*-DSB isomer was separated from the mixture by column chromatography (silica gel, 85 hexane: 15 chloroform) and further purified by recrystallization. The *trans,trans*-DSB sample of $5 \times 10^{-5}$ M in *n*-hexane was prepared for laser experiments in a flow cell, and the flow rate was adjusted to be fast enough to avoid excitation of the same molecule by two sequential pump pulses. Because the isomerized product, *cis,trans*-DSB, was constantly formed during the laser experiments, the fraction of the *trans,trans*-DSB isomer was monitored regularly by HPLC and assured to be greater than 97%.

The details of the ultrafast laser system and transient absorption setup have been described elsewhere.[11] Briefly, a 1 kHz train of 130 fs laser pulses with 1 mJ pulse energy, centered at 800 nm, serves as the light source for the following

* Corresponding authors. E-mail: atmyh@ntu.edu.tw (M.H.); jkwang@ccms.ntu.edu.tw (J.-K.W.).
[†] Department of Chemistry, National Taiwan University.
[‡] Center for Condensed Matter Sciences, National Taiwan University.
[§] Academia Sinica.

10.1021/jp0652897 CCC: $37.00 
Published on Web 01/18/2007

wavelength conversion processes. The pump beam is generated by the fourth-harmonic-generation of the signal output from a home-built optical parametric amplifier and its wavelength can be varied from 300 to 380 nm.[15] The supercontinuum probe beam (700−900 nm) is generated by focusing the 800 nm laser pulse in a sapphire window. The polarization of the probe is selected to be 45° to that of the pump. After overlapping with the pump beam in the sample flow cell, the transmitted probe beam is separated into two components with polarizations parallel and perpendicular to that of the pump beam ($I_{\parallel}$ and $I_{\perp}$). These two probe components are dispersed by a 32 cm monochromator to select a specific probe wavelength ($\lambda_{pr}$) with 3 nm spectral bandwidth and then detected simultaneously by two separate photodiodes. In a phase-locked detection scheme, the pump-induced variation of the two detected probe signals, $\Delta I_{\parallel}(\Delta t,\lambda_{pr})$ and $\Delta I_{\perp}(\Delta t,\lambda_{pr})$, are extracted by two independent lock-in amplifiers, where $\Delta t$ is the pump−probe time delay provided by a computer-controlled delay stage on the pump beam path. The polarization-dependent throughput of all optical components after the sample cell and the responses of two photodiodes with corresponding lock-in amplifiers are carefully calibrated for each probe wavelength. Both isotropic and anisotropic components of the transient absorption data at each probe wavelength can be accordingly derived. The transient absorption anisotropy is derived from the following relation:

$$r(\Delta t,\lambda_{pr}) = [\Delta I_{\parallel}(\Delta t,\lambda_{pr}) - \Delta I_{\perp}(\Delta t,\lambda_{pr})]/\{[\Delta I_{\parallel}(\Delta t,\lambda_{pr}) + 2\Delta I_{\perp}(\Delta t,\lambda_{pr})]\} \quad (1)$$

The isotropic component of transient absorption is derived according to

$$\Delta A_{iso}(\Delta t,\lambda_{pr}) \propto -[\Delta I_{\parallel}(\Delta t,\lambda_{pr}) + 2\Delta I_{\perp}(\Delta t,\lambda_{pr})] \quad (2)$$

In the excitation energy dependence measurements, the probe wavelength is selected to be 700 nm because it provides a large excited-state absorption cross section and therefore the kinetic parameters can be readily extracted.[11]

In our computational effort, the geometry of the electronically ground state of *trans,trans*-DSB is fully optimized using density functional theory (DFT) at B3LYP level[16−26] with the 6-311G* Gaussian basis set. On the basis of the optimized ground-state geometry, we used ZINDO/S method[27,28] to calculate the electronic excitation energies from ground state ($S_0$) to excited states ($S_n$), as well as the corresponding oscillator strengths and transition dipole moments. The first excited-state ($S_1$) geometry is subsequently optimized at configuration interaction singles (CIS)[29] with 6-31G* and 6-31+G* starting with the optimized $S_0$ geometry. The molecular geometry of the $S_1$ state is estimated on the basis of the 6-31G* calculation result.

### 3. Results and Discussion

On the basis of our previous study of excited-state dynamics of *trans,trans*-DSB,[11] we here propose a dynamical model as shown in Figure 1. The UV-pump pulse excites the molecule from the $S_0$ state to the $S_1$ state with the absorption cross-section of $\sigma_{01}$. The subsequent intramolecular vibrational redistribution (IVR) process is completed within our time resolution and quickly equilibrates the excitation energy of Franck−Condon active modes with all other vibrational modes. This was confirmed by the transient absorption experiment performed with the pump wavelength tuned to the 0−0 electronic transition. The vibrationally equilibrated population in the $S_1$ state then undergoes a nonradiative transition to the X state with a rate constant of ∼0.1 $ps^{-1}$ ($k_1$) and subsequently decays in ∼2 ns ($k_X$). Over the range of the selected probe wavelengths (from 700 to 760 nm), the observed excited-state absorption is therefore composed of two components that are associated with two Franck−Condon regions: one is from the $S_1$ state with the corresponding excited-state absorption cross-section $\sigma_{1n}$ and the other one is from the X state with the corresponding $\sigma_{Xm}$. The pump-induced probe absorption at $\lambda_{pr} \geq 740$ nm at early time (<10 ps) is mainly due to the excited-state absorption of the $S_1$ state, and the observed 10 ps decay component reflects the decrease of the initially excited population in the $S_1$ state. In comparison, the absorption from the X state dominates at $\lambda_{pr} \leq 720$ nm. The 10 ps rising component in transient absorption represents the population transferred from the $S_1$ state to the X state. The vibrational relaxation in the $S_1$ state cannot account for the 10 ps dynamical behaviors because they are still observable when the pump wavelength is tuned to the 0−0 electronic transition.[11]

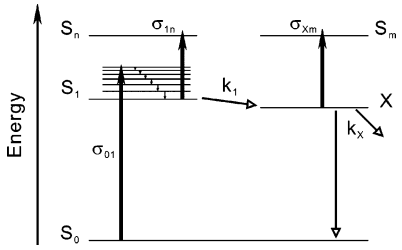


**Figure 1.** Schematic photoexcitation kinetic diagram of *trans,trans*-DSB. $S_0$, $S_1$, $S_n$ and $S_m$ represent singlet electronic states, and X indicates an intermediate state. The $\sigma_{ij}$ represents the absorption cross-section for $i \rightarrow j$ electronic transition. $k_1$ is the population transfer rate from $S_1$ to X; $k_X$ indicates the population decay rate of the X state.

**TABLE 1: Characteristics of Electronic Transitions of *trans,trans*-DSB Calculated by ZINDO/S[a]**

| | $\mu_x$ (au) | $\mu_y$ (au) | $\mu_z$ (au) | $f$ | $\Delta E$ (eV) | $\lambda$ (nm) |
|---|---|---|---|---|---|---|
| $S_0 \rightarrow S_1$ | −4.7818 | 0.2843 | 0.0002 | 1.8870 | 3.3567 | 369.37 |
| $S_1 \rightarrow S_2$ | 0.0000 | 0.0000 | 0.0000 | 0.0000 | 0.7621 | 1626.88 |
| $S_1 \rightarrow S_3$ | 0.8884 | 0.0292 | −0.0003 | 0.0161 | 0.8328 | 1488.77 |
| $S_1 \rightarrow S_4$ | 0.0002 | 0.0000 | 0.0000 | 0.0000 | 0.9913 | 1250.72 |
| $S_1 \rightarrow S_5$ | 0.0933 | −0.4376 | 0.0010 | 0.0049 | 0.9933 | 1248.21 |
| $S_1 \rightarrow S_6$ | 0.0000 | 0.0000 | 0.0000 | 0.0000 | 1.4924 | 830.77 |
| $S_1 \rightarrow S_7$ | 6.1793 | −0.0048 | −0.0002 | 1.4744 | 1.5761 | 786.65 |
| $S_1 \rightarrow S_8$ | 0.0000 | −0.0001 | 0.0000 | 0.0000 | 1.8957 | 654.03 |
| $S_1 \rightarrow S_9$ | 0.0431 | 0.0353 | 0.0003 | 0.0002 | 2.0180 | 614.39 |

[a] $\{\mu_x, \mu_y, \mu_z\}$ are Cartesian components of the transition dipole moment in atomic units, $f$ is the oscillator strength, $\Delta E$ is its transition energy, and $\lambda$ is the corresponding excitation wavelength. The geometry used for the calculation is the ground-state optimization structure obtained with B3LYP/6-311G**.

The understanding of the observed excited-state absorption characteristics of *trans,trans*-DSB can be facilitated by the ZINDO/S calculation. Table 1 presents the calculation results that consist of orientations of electronic transition dipole moments, corresponding oscillator strengths, excitation energies, and corresponding excitation wavelengths. The wavelength corresponding to $S_0 \rightarrow S_1$ is calculated to be 369 nm, which is consistent with the steady-state absorption spectrum.[10] For excited-state absorption, the most probable transition from $S_1$ is $S_1 \rightarrow S_7$, which is located at 787 nm with an oscillator strength much stronger than those for nearby possible transitions. This predicted excited-state absorption wavelength is consistent with the excited-state absorption spectra observed at the early time delay. Finally, the orientation information of electronic transition

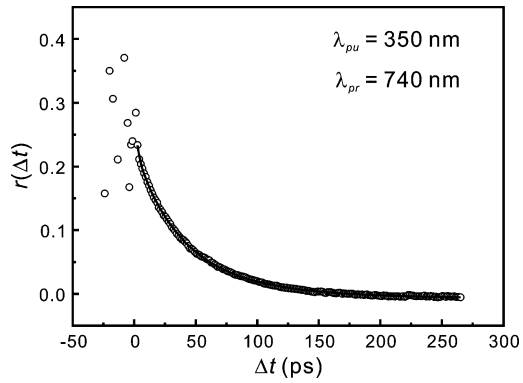


**Figure 2.** Typical anisotropy decay curve of transient absorption signal of *trans,trans*-DSB. The pump and probe wavelengths are 350 and 740 nm, respectively. The open circles represent the experimental data, and the solid line indicates the fitted curve.

dipole moments provides a consistency check for the proposed kinetic model in the analysis of transient absorption anisotropy (vide infra).

On the basis of the proposed kinetic model (Figure 1), we derived a dynamical equation for describing the excited-state anisotropy:

$$r(\Delta t,\lambda_{pr}) = r_e(\Delta t,\lambda_{pr})\cdot R_D(\Delta t) \quad (3)$$

where $r_e(\Delta t,\lambda_{pr})$ represents the dynamical electronic anisotropy related to the population kinetics of *trans,trans*-DSB and $R_D(\Delta t)$ represents the anisotropy relaxation due to its molecular rotational motion. In this description, two assumptions have been made. First, the excited-state population kinetics is decoupled from the molecular rotational motion in the spirit of Born−Oppenheimer approximation. Second, rotational diffusion is assumed to be the only anisotropy relaxation mechanism of nuclear motion in the limit of the rigid rotor approximation. That is, the conformation of *trans,trans*-DSB is not altered in the time scale of interest. In this case, *trans,trans*-DSB is a rigid rodlike symmetric rotor (prolate) with two rotational axes and therefore has two distinct diagonal elements of the rotational diffusion tensor in the molecular-coordinate system. One axis is along the $\pi$−conjugated backbone and the other one is perpendicular to it. $R_D(\Delta t)$ is thus reduced to[30]

$$R_D(\Delta t) = \frac{1}{4}\exp(-6D_\perp\Delta t) + \frac{3}{4}\exp[-(2D_\perp + 4D_{||})\Delta t] \quad (4)$$

where $D_\perp$ and $D_{||}$ correspond to the rotational diffusion coefficients of tumbling and spinning motions, respectively. Dynamical electronic anisotropy, $r_e$, is given by[31]

$$r_e(\Delta t,\lambda_{pr}) = \frac{(3\cos^2\theta_{10} - 1)\rho_{11}(\Delta t,\lambda_{pr}) + \beta\cdot(3\cos^2\theta_{X0} - 1)\rho_{XX}(\Delta t,\lambda_{pr})}{5[\rho_{11}(\Delta t,\lambda_{pr}) + \beta\cdot\rho_{XX}(\Delta t,\lambda_{pr})]} \quad (5)$$

where $\theta_{10}$ ($\theta_{X0}$) is the angle between $\bar{\mu}_{1n}$ ($\bar{\mu}_{Xm}$) and $\bar{\mu}_{01}$, $\beta$ represents $|\bar{\mu}_{Xm}\}/|\bar{\mu}_{1n}|^2$, which is proportional to $\sigma_{Xm}/\sigma_{1n}$, and $\rho_{11}$ ($\rho_{XX}$) is the population in the $S_1$ (X) state. With their kinetics extracted from the isotropic transient absorption components,[11] eqs 3−5 are used to fit the anisotropic transient absorption data. The transient absorption anisotropy for $\lambda_{pu} = 350$ nm and $\lambda_{pr} = 740$ nm, shown in Figure 2, is a typical example. Notice that that the fitted curve is in good agreement with the experimental data. The extracted parameters for four different probe wavelengths in the excited-state absorption spectrum (700, 720, 740 and 760 nm) are listed in Table 2, from which four facts can be drawn. First, the two extracted rotational diffusion coefficients, $D_\perp$ and $D_{||}$, are 2.1 and 6.0 GHz, respectively, and do not vary with the probe wavelengths. Second, all $\theta_{10}$ are consistently around 160° for different probe wavelengths. Third, the extracted $\beta$ values remain constant for the four probe wavelengths. Finally, $\theta_{X0}$ decreases from 36° to 23° as the probe wavelength varies from 700 to 760 nm.

**TABLE 2: Fitted Results of Anisotropy Dynamics of *trans,trans*-DSB Based on Rigid Rotor Model[a]**

| $\lambda_{pr}$ (nm) | $\theta_{10}$ (deg) | $\theta_{X0}$ (deg) | $\beta$ | $D_\perp$ (GHz) | $D_{||}$ (GHz) |
|---|---|---|---|---|---|
| 760 | 165.2 ± 2.3 | 36.0 ± 0.4 | 10.21 ± 1.23 | 2.2 ± 0.19 | 6.1 ± 0.38 |
| 740 | 153.5 ± 0.4 | 32.8 ± 0.1 | 10.28 ± 0.43 | 2.1 ± 0.05 | 5.9 ± 0.09 |
| 720 | 151.2 ± 0.3 | 29.2 ± 0.2 | 10.17 ± 0.38 | 2.1 ± 0.04 | 5.8 ± 0.09 |
| 700 | 155.2 ± 0.9 | 23.3 ± 0.3 | 10.24 ± 0.77 | 2.1 ± 0.08 | 5.9 ± 0.13 |
| | 176.6[b] | | | 2.9[c] | 6.1[c] |

[a] $\theta_{10}$ ($\theta_{X0}$) is the angle between $\mu_{01}$ and $\mu_{17}$ ($\mu_{Xm}$). $\beta$ represents $|\mu_{Xm}/\mu_{17}|^2$, and $D_{||}$ and $D_\perp$ are the rotational diffusion constants parallel with and perpendicular to the long axis of the prolate-shaped *trans,trans*-DSB, respectively. [b] The value is estimated from the ZINDO/S results shown in Table 1. [c] The value is estimated from the ground-state molecular structure calculated on the basis of the CIS with 6-31G*.

In the approximation of a rigid ellipsoid, the two rotational diffusion coefficients can be estimated according to the following two equations:[32]

$$D_\perp = \frac{3}{2}\frac{\delta[(2\delta^2 - 1)W - \delta]}{(\delta^4 - 1)}D_S \quad (6)$$

and

$$D_{||} = \frac{3}{2}\frac{\delta(\delta - W)}{(\delta^2 - 1)}D_S \quad (7)$$

where $D_S = k_BT/6V\eta$, $W = \ln[\delta + (\delta^2 - 1)^{1/2}]/(\delta^2 - 1)^{1/2}$, $D_S$ is the rotational diffusion coefficient of a sphere with an equivalent volume $V$ to the ellipsoidal rotor, $\delta$ is the axial ratio of the rotor ($\delta > 1$ for prolate), and $\eta$ represents the solvent viscosity which is $3.26 \times 10^{-4}$ kg·m$^{-1}$·s$^{-1}$ for *n*-hexane at room temperature.[33] Based on the optimized structure from the theoretical calculation, the calculated radii of the long and short axis of the ellipsoid are 9.17 and 2.49 Å, respectively, yielding the two corresponding rotational coefficients: $D_\perp$= 2.9 GHz and $D_{||}$ = 6.1 GHz. The agreement between the fitted results and the estimated values therefore supports the rigid rotor approximation and suggests that the molecular conformation change is insignificant in the time scale of rotational diffusion relaxation.

In our calculation, it is found that both $\bar{\mu}_{01}$ and $\bar{\mu}_{17}$ align approximately along the $\pi$−conjugated backbone of *trans,trans*-DSB. The angle between $\bar{\mu}_{17}$ and $\bar{\mu}_{01}$ ($\theta_{10}$) is calculated to be 176.6°, which is quite close to the experimentally deduced values from the anisotropy analysis (Table 1). This agreement further confirms that the $S_1 \rightarrow S_7$ transition dominates the contribution for $\lambda_{pr} \geq 740$ nm and the observed decay in the transient absorption signal represents the population transfer out of the $S_1$ state. It is noticed that all the deduced $\beta$ ($= |\bar{\mu}_{Xm}/\bar{\mu}_{1n}|^2$) values approach 10, suggesting that the proposed kinetic model can consistently explain all the excited-state isotropic and anisotropic behaviors of *trans,trans*-DSB. Finally, the observation that $\theta_{X0}$ varies with the probe wavelength from 36° to 23° needs further discussion. Although the transition dipole is fixed in the rigid rotor approximation, single-bond rotation in the $\pi$−conjugated backbone of *trans,trans*-DSB may sig-

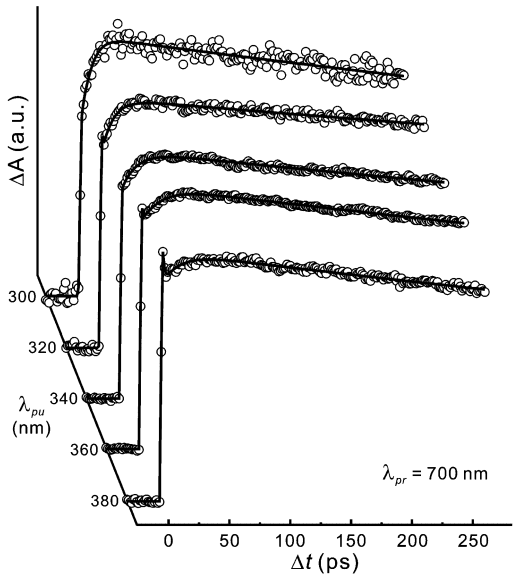


**Figure 3.** Pump wavelength dependence of isotropic transient absorption at probe wavelength of 700 nm. The open circles represent the experimental data, and the solid lines indicate the fitted curves.

nificantly affect the direction of the transition dipole moment but maintain its moment of inertia. The different $\theta_{X0}$ values at various probe wavelengths are probably due to such a distribution of rotamers with different phenyl/vinyl torsional angles in the X state. In sum, both isotropic[11] and anisotropy relaxation studies indicate the existence of the intermediate X state, which is in great contrast to the case of *trans*-stilbene. On the basis of the observation of fluorescence lifetime (1.8 ns) and photoisomerization quantum yield ($8 \times 10^{-4}$),[10] this X state apparently serves as the precursor for the photoisomerization process.

To unveil the nature of the coupling between the $S_1$ and X states, we monitored the population transfer rate ($k_1$) as a function of the excess energy in the $S_1$ state by varying the pump wavelength. As presented previously,[11] intramolecular vibrational redistribution (IVR) in the $S_1$ state of *trans,trans*-DSB occurs almost instantaneously within the pump pulse duration. This excess energy is expected to establish an intramolecular temperature before the population transfer process takes place. The variation of the pump wavelength thus results in the alteration of the internal temperature in the excited state. Figure 3 shows the isotropic transient absorption data at $\lambda_{pr} =$ 700 nm for five different pump wavelengths as illustrating examples. Notice that the 10 ps dynamics becomes faster with a decreasing of the pump wavelength. The intramolecular temperature $T_{int}$ resulted from the ultrafast equilibration of the excess energy $\langle E_{ex} \rangle$[34] among all 114 internal vibrational modes can be evaluated from the ensemble average,

$$\langle E_{ex} \rangle = \sum_{\nu} \frac{\hbar\omega_v}{e^{\hbar\omega_\nu / k_B T_{int}} - 1} \qquad (8)$$

where $\omega_v$ is the radial vibrational frequency of the $\nu$th mode. The dependence of $k_1$ on the extracted $T_{int}$ is shown in Figure 4 for the pump wavelength varied from 300 to 370 nm. To analyze this dependence, we invoke a model of temperature effect on radiationless transition:[35]

$$k_1/k_1^0 = 1 + f_1 \exp(-\hbar\omega_1/k_B T_{int}) \qquad (9)$$

where $k_1^0$ is the rate constant at $T_{int} = 0$ K, $\omega_1$ is the effective vibrational mode responsible for this $k_1$ nonradiative process,

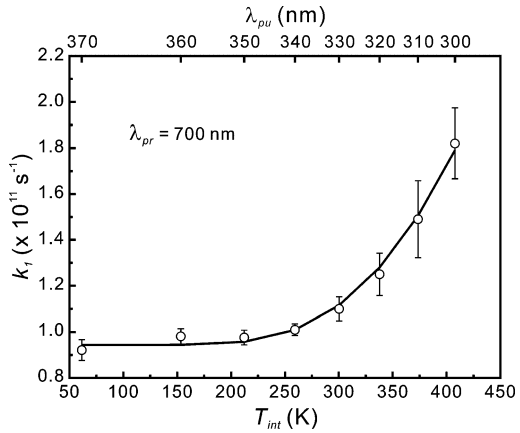


**Figure 4.** Intramolecular temperature dependence of the population transfer rate from $S_1$ to X, $k_1$. The error bar in each data point corresponds to the fitting error of the transient absorption data. The solid line represents the fitted curve by eq 9.

and $f_1$ is the pre-exponential factor related to the changes in the normal coordinate and frequency in the equilibrium configuration when the process occurs. $k_1^0$ is extracted to be $9.2 \times 10^{10}$ $s^{-1}$. This fast population transfer process also implies that the X state is a singlet state of presumably different geometry relative to the $S_1$ state. The fitted $\omega_1$ and $f_1$ are $1270 \pm 36$ $cm^{-1}$ and 84.6, respectively. According to our CIS calculation, the optically active modes of ground-state absorption lie within 1200−1300 $cm^{-1}$ and they are associated with the out-of-plain motion of the benzene ring near 1000 $cm^{-1}$, which might be related to the rotation about the internal phenyl−vinyl single bonds. Notice that the extracted vibrational mode ($\omega_1$) responsible for this 10 ps nonradiative process may not be unique, indicating that there are probably several modes with similar frequencies that contribute to the $f_1$ factor. Moreover, the deduced $\omega_1$ mode (or modes) should be also related to the rotamer distribution in the X state caused by different amplitudes of internal phenyl−vinyl dihedral angles, which is suggested by the observation that the transition dipole orientation of the X-state absorption gradually varies with the probe wavelength (Table 2).

The origin of this X state is worthy of more discussion. It is known that for linear centrosymmetric conjugated molecules, their two lowest excited states ($1^1B_u^-$ and $2^1A_g^+$) have different symmetry properties such that the transition $1^1B_u^- \rightarrow 1^1A_g^+$ is optically allowed but the transition $2^1A_g^+ \rightarrow 1^1A_g^+$ is forbidden, where the $1^1A_g^+$ state is the highest occupied molecular orbital.[36] Furthermore, the proximity between the $1^1B_u^-$ and $2^1A_g^+$ states may induce strong vibronic mixing, making possible the observation of emission from the $2^1A_g^+$ state.[37] For example, the fluorescence spectrum of *all-trans*-1,6-diphenyl-1,3,5-hexatriene (*all-trans*-DPH) in solution has been resolved into two components from $1^1B_u^-$ and $2^1A_g^+$, respectively.[38] In comparison, on the basis of our calculation, the oscillator strength of the $S_0 \rightarrow S_1$ transition of *trans,trans*-DSB is much larger than that of the $S_0 \rightarrow S_2$ transition. The $S_2$ state is thus unlikely the X state. Our ultrafast anisotropy study, however, identifies the different electronic nature of the X state from the $S_1$ state. Is it possible that the vibronic mixing between $S_1$ and $S_2$ or another nearby electronic state is responsible for the formation of this X state and is the origin of the 10 ps population transfer process? Further theoretical investigations are required to answer this question and to unveil the role of the X state in photoisomerization.

## 4. Conclusions

A kinetic model has been proposed to describe the ultrafast nonradiative 10 ps dynamics ($k_1$) of *trans*,*trans*-DSB in the $S_1$ state. An intermediate X state that plays a critical role in this model is proposed to be responsible for the observed 10 ps dynamics, representing the efficient population transfer from the $S_1$ state to the X state. A rigid rotor model has been used to analyze the anisotropy data. The deduced rotational diffusion coefficients and transition dipole orientation of the $S_1$-state absorption are consistent with the theoretically estimated values. The observation that the ratio of two transition dipole moments ($S_1 \rightarrow S_7$ and $X \rightarrow S_m$) is invariant of the probe wavelength further supports the existence of the X state. These consistent results obtained over all the probe wavelengths show that the anisotropy study combined with the isotropic transient absorption study confirms this kinetic model. The characteristics of this population transfer process have been further investigated by the pump-dependent transient absorption measurements. The corresponding $k_1$ has been observed as a function of the excess energy. A weak coupling model is proposed to analyze this relationship, yielding a specific vibrational mode of $\sim$1270 $cm^{-1}$ responsible for the 10 ps nonradiative process. More detailed theoretical investigation on this issue to elucidate the characteristics of the X state is suggested and is currently under way.

**Acknowledgment.** We thank the financial supports from the National Science Council (Grant No. 95-2745-M-002-010 and 95-2112-M-002-022) and Academia Sinica in Taiwan, and the National Center for High-Performance Computing for providing the CPU time and computing resources.

## References and Notes

(1) Burroughes, J. H.; Bradley, D. D. C.; Brown, A. R.; Marks, R. N.; Mackay, K.; Friend, R. H.; Burns, P. L.; Holmes, A. B. *Nature* **1990**, *347*, 539.

(2) Rothberg, L. J.; Yan, M.; Galvin, M. E.; Kwock, E. W.; Miller, T. M.; Papadimitrakopoulos, F. *Synth. Metals* **1996**, *80*, 41.

(3) Saltiel, J.; Sun, Y.-P. In *Photochromism, Molecules and Systems*; Dürr, H., Bouas-Laurent, H., Eds.; Elsevier: Amsterdam, 1990; pp 64−164.

(4) Waldeck, D. H. *Chem. Rev.* **1991**, *91*, 415 and references therein.

(5) Bredas, J. L.; Cornil, J.; Beljonne, D.; dos Santos, D. A.; Shuai, Z. *Acc. Chem. Res.* **1999**, *32*, 267.

(6) Sandros, K.; Sundahl, M.; Wennerström, O.; Norinder, U. *J. Am. Chem. Soc.* **1990**, *112*, 3082.

(7) Sundahl, M.; Wennerström, O.; Sandros, K.; Arai, T.; Tokumaru, K. *J. Phys. Chem.* **1990**, *94*, 6731.

(8) Anger, I.; Sundahl, M.; Wennerström, O.; Sandros, K.; Arai, T.; Tokumaru, K. *J. Phys. Chem.* **1992**, *96*, 7027.

(9) Sandros, K.; Sundahl, M. *J. Phys. Chem.* **1994**, *98*, 5705.

(10) Marri, E.; Pannacci, D.; Galiazzo, G.; Mazzucato, U.; Spalletti, A. *J. Phys. Chem. A* **2003**, *107*, 11231.

(11) Hsu, F.-C.; Lin, S. H.; Wang, J.-K. *Chem. Phys. Lett.* **2005**, *411*, 103.

(12) Greene, B. I.; Hochstrasser, R. M.; Weismann, R. B. *Chem. Phys. Lett.* **1979**, *62*, 427.

(13) Doany, F. E.; Greene, B. I.; Hochstrasser, R. B. *Chem. Phys. Lett.* **1980**, *75*, 206.

(14) Campbell, T. W.; McDonald, R. N. *J. Org. Chem.* **1959**, *24*, 1246.

(15) Wang, J.-C.; Wang, J.-K. *J. Opt. Soc. Am. B* **2004**, *21*, 45.

(16) Dirac, P. A. M. *Proc. R. Soc. (London) A* **1929**, *123*, 714.

(17) Slater, J. C. *Phys. Rev.* **1951**, *81*, 385.

(18) Vosko, S. H.; Wilk, L.; Nusair, M. *Can. J. Phys.* **1980**, *58*, 1200.

(19) Becke, A. D. *Phys. Rev. A* **1988**, *38*, 3098.

(20) Lee, C.; Yang, W.; Parr, R. G. *Phys. Rev. B* **1988**, *37*, 785.

(21) Becke, A. D. *J. Chem. Phys.* **1993**, *98*, 5648.

(22) Frisch, M. J.; Trucks, G. W.; Schlegel, H. B.; Scuseria, G. E.; Robb, M. A.; Cheeseman, J. R.; Montgomery, J. A., Jr.; Vreven, T.; Kudin, K. N.; Burant, J. C.; Millam, J. M.; Iyengar, S. S.; Tomasi, J.; Barone, V.; Mennucci, B.; Cossi, M.; Scalmani, G.; Rega, N.; Petersson, G. A.; Nakatsuji, H.; Hada, M.; Ehara, M.; Toyota, K.; Fukuda, R.; Hasegawa, J.; Ishida, M.; Nakajima, T.; Honda, Y.; Kitao, O.; Nakai, H.; Klene, M.; Li, X.; Knox, J. E.; Hratchian, H. P.; Cross, J. B.; Bakken, V.; Adamo, C.; Jaramillo, J.; Gomperts, R.; Stratmann, R. E.; Yazyev, O.; Austin, A. J.; Cammi, R.; Pomelli, C.; Ochterski, J. W.; Ayala, P. Y.; Morokuma, K.; Voth, G. A.; Salvador, P.; Dannenberg, J. J.; Zakrzewski, V. G.; Dapprich, S.; Daniels, A. D.; Strain, M. C.; Farkas, O.; Malick, D. K.; Rabuck, A. D.; Raghavachari, K.; Foresman, J. B.; Ortiz, J. V.; Cui, Q.; Baboul, A. G.; Clifford, S.; Cioslowski, J.; Stefanov, B. B.; Liu, G.; Liashenko, A.; Piskorz, P.; Komaromi, I.; Martin, R. L.; Fox, D. J.; Keith, T.; Al-Laham, M. A.; Peng, C. Y.; Nanayakkara, A.; Challacombe, M.; Gill, P. M. W.; Johnson, B.; Chen, W.; Wong, M. W.; Gonzalez, C.; Pople, J. A. *Gaussian 03*, revision C.02; Gaussian, Inc.: Wallingford, CT, 2004.

(23) Ahlrichs, R.; Bär, M.; Häser, M.; Horn, H.; Kölmel, C. *Chem. Phys. Lett.* **1989**, *162*, 165.

(24) Treutler, O.; Ahlrichs, R. *J. Chem. Phys.* **1995**, *102*, 346.

(25) For the ground-state and excited-state geometry optimizations, correlation functionals VWN(V) and VWN(VI) were used, respectively. Here VWN(V) is also used in the G03 package. Note that a structure of the excited state could not be obtained using VWN(V).

(26) Schäfer, A.; Huber, C.; Ahlrichs, R. *J. Chem. Phys.* **1994**, *100*, 5829.

(27) Bacon, A. D.; Zerner, M. C. *Theo. Chim. Acta* **1979**, *53*, 21.

(28) Hanson, L. K.; Fajer, J.; Thompson, M. A.; Zerner, M. C. *J. Am. Chem. Soc.* **1987**, *109*, 4728.

(29) Foresman, J. B.; Head-Gordon, M.; Pople, J. A.; Frisch, M. J. *J. Phys. Chem.* **1992**, *96*, 135.

(30) Fleming, G. R. *Chemical Applications of Ultrafast Spectroscopy*; Oxford University Press: Oxford, U.K., 1986; pp 128−130.

(31) Hayashi, M.; Yang, T.-S.; Yu, J.; Mebel, A.; Chang, R.; Lin, S. H.; Robtsov, I. V.; Yoshihara, K. *J. Phys. Chem. A* **1998**, *102*, 4256.

(32) Shimizu, H. *J. Chem. Phys.* **1962**, *37*, 765.

(33) *Handbook of Chemistry and Physics*, 69th ed.; Weast, R. C., Ed.; CRC Press: Boca Raton, FL, 1988−1989; pp F41ff.

(34) The $E_{0-0}$ (0−0 electronic transition energy, 26 846 $cm^{-1}$) is determined at the crossing of $\bar{\alpha}(\omega)$ and $\bar{I}_F(\omega)$, where $\bar{\alpha}(\omega) = \alpha(\omega)/\int[\alpha(\omega)/\omega]\, d\omega$, $\bar{I}_F(\omega) = I_F(\omega)/\int[I_F(\omega)/\omega^3]\, d\omega$, $\alpha(\omega)$ is the absorption spectrum, and $I_F(\omega)$ is the fluorescence spectrum.

(35) Lin, S. H. *J. Chem. Phys.* **1972**, *56*, 2648.

(36) Brédas, J.-L.; Cornil, J.; Beljonne, D.; Dos, Santos, D. A.; Shuai, Z. *Acc. Chem. Res.* **1999**, *32*, 267.

(37) Itoh, T. *J. Chem. Phys.* **2005**, *123*, 064302 and references therein.

(38) Turek, A. M.; Krishnamoorthy, G.; Sears, D. F., Jr.; Garcia, I.; Dmitrenko, O.; Saltiel, J. *J. Phys. Chem. A* **2005**, *109*, 293.